Self-generated Template Pathway to High-Surface-Area Zinc Aluminate Spinel with Mesopore Network from a Single-Source Inorganic Precursor

Lu Zou, Feng Li,* Xu Xiang, David G. Evans, and Xue Duan

State Key Laboratory of Chemical Resource Engineering, P.O. Box 98, Beijing University of Chemical Technology, Beijing 100029, P.R. China

Received March 14, 2006. Revised Manuscript Received July 18, 2006

Zinc aluminate spinels ($ZnAl_2O_4$) with mesopore networks and unusually high specific surface areas have been prepared through a self-generated template pathway using a single-source Zn−Al layered double hydroxide as precursor. This strategy involves calcination of the molecular precursor at 500 °C or above, followed by selective leaching of the self-generated zinc oxide template from the resultant calcined products. The specific surface area of $ZnAl_2O_4$ obtained after calcination at 500 °C is as high as 253 $m^2\ g^{-1}$ and then decreases gradually with calcination temperature. The templating effect of self-generated ZnO is the essential factor directing the formation of the present high-surface-area $ZnAl_2O_4$ spinels with interconnected mesopore networks. Since the precursor has a uniform distribution of metal cations on an atomic level, the formation of spinel requires a low temperature and short calcination time. Further, through photocatalytic investigation, these as-prepared $ZnAl_2O_4$ spinels displayed better abilities to photodecompose phenol under UV irradiation due to their higher surface areas structure, compared to $ZnAl_2O_4$ sample prepared by the conventional solid-state method.

Introduction

Inorganic materials with high specific surface areas have found increasing application in areas such as heterogeneous catalysts, functional ceramics, adsorbents, and sensors.[1] In principle, high surface area may be introduced either by dividing the bulk material to the nanometer scale or by making it porous.[2] At present, several techniques based on sol−gel processing,[3] microemulsions,[4] and templating[2] are available for producing such materials. Of these, templating is a versatile pathway that has attracted considerable attention in recent years. This is because the templating approach provides an unprecedented ability to tailor the structural and textural properties, such as pore size distribution and overall porosity, along with the external shape and size of the sample particles.[5] Schüth's group has investigated the use of activated carbon or carbon aerogels as hard templates for the synthesis of several high-surface-area metal oxide materials.[1a,6] Recently, Valdés-Solís et al.[7] have prepared high-surface-area perovskite- and spinel-type complex oxides using porous silica xerogel as hard template. However, many templates have drawbacks in terms of affordability and/or versatility and the design of new types of templates is currently an area of major activity.

Transition metal spinels are an important class of functional inorganic materials. For example, zinc aluminate ($ZnAl_2O_4$), also referred to as spinel-type Zn−Al complex oxide, has a wide range of applications. It mainly serves as catalysts and catalyst supports in synthesis, dehydrogenation, dehydrocyclization, hydrogenation, dehydration, selective catalytic reduction, isomerization, and combustion processes.[8] Besides, it is a wide band gap semiconductor (3.8 eV)[9] that can be used as a transparent conductor,[10] dielectric material,[11] optical material,[12] and sensor.[13] If spinels are prepared by typical ceramic processes involving calcination of physical mixtures of precursors, considerably elevated temperatures

* Corresponding author. Tel.: 8610-64451226. Fax: 8610-64425385. E-mail: lifeng_70@163.com (F. Li).

(1) (a) Schwickardi, M.; Johann, T.; Schmidt, W.; Schüth, F. *Chem. Mater.* **2002**, *14*, 3913. (b) Kemnitz, E.; Groβ, U.; Rüdiger, S.; Shekar, C. S. *Angew. Chem., Int. Ed.* **2003**, *42*, 4251.
(2) Schüth, F. *Angew. Chem., Int. Ed.* **2003**, *42*, 3604.
(3) (a) Brinker, C. J.; Scherer, G. W. *Sol-Gel Science*; Academic Press: Boston, 1990. (b) Zayat, M.; Levy, D. *Chem. Mater.* **2000**, *12*, 2763.
(4) (a) Bumajdad, A.; Zaki, M. I.; Eastoe, J.; Pasupulety, L. *Langmuir* **2004**, *20*, 11223. (b) Teng, F.; Xu, J.; Tian, Z.; Wang, J.; Xu, Y.; Xu, Z.; Xiong, G.; Lin, L. *Chem. Commun.* **2004**, 1858.
(5) Caruso, R. A. *Top. Curr. Chem.* **2003**, *226*, 91.
(6) (a) Li, W.; Lu, A.; Schmidt, W.; Schüth, F. *Chem. Eur. J.* **2005**, *11*, 1658. (b) Li, W.; Lu, A.; Weidenthaler, C.; Schüth, F. *Chem. Mater.* **2004**, *16*, 5676.
(7) Valdés-Solís, T.; Marban, G.; Fuertes, A. B. *Chem. Mater.* **2005**, *17*, 1919.
(8) (a) Shen, S.; Hidajat, K.; Yu, L. E.; Kawi, S. *Adv. Mater.* **2004**, *16*, 541. (b) Roesky, R.; Weiguny, J.; Bestgen, H.; Dingerdissen, U. *Appl. Catal. A* **1999**, *176*, 213. (c) Le Pelter, F.; Chaumette, P.; Saussey, J.; Bettahar, M. M.; Lavalley, J. C. *J. Mol. Catal. A: Chem.* **1997**, *122*, 131. (d) Valenzuela, M. A.; Aguilar, A.; Bosch, P.; Armendariz, H.; Salas, P.; Montoya, A. *Catal. Lett.* **1992**, *15*, 179. (e) Chen, L.; Sun, X.; Liu, Y.; Zhou, K.; Li, Y. *J. Alloys Compd.* **2004**, *376*, 257. (f) Aguilar-Ríos, G.; Valenzuela, M. A; Salas, P.; Armendáriz, H.; Bosch, P.; Del Toro, G.; Silva, R.; Bertín, V.; Castillo, S.; Ramírez-Solís, A.; Schifter, I. *Appl. Catal. A* **1995**, *127*, 65. (h) Grabowska, H.; Mita, W.; Trawczyski, J.; Wrzyszcz, J.; Zawadzki, M. *Appl. Catal. A* **2001**, *220*, 207. (i) Kienle, C.; Schinzer, C.; Lentmaier, J.; Schaal, O.; Kemmlersack, S. *Mater. Chem. Phys.* **1997**, *49*, 211.
(9) Sampath, S. K.; Cordaro, J. F. *J. Am. Ceram. Soc.* **1998**, *81*, 649.
(10) García-Hipólito, M.; Guzmán-Mendoza, J.; Martínez, E.; Alvarez-Fregoso, O.; Falcony, C. *Phys. Status Solidi A* **2004**, *201*, 1510.
(11) Van der Laag, N. J.; Snel, M. D.; Magusin, P. C. M. M.; de With, G. *J. Eur. Ceram. Soc.* **2004**, *24*, 2417.
(12) Mathur, S.; Veith, M.; Haas, M.; Shen, A.; Lecerf, N.; Huch, V.; Hufner, S.; Haberkorn, R.; Beck, H. P.; Jilavi, M. *J. Am. Ceram. Soc.* **2001**, *84*, 1921.
(13) Matsui, H.; Xu, C.; Tateyama, H. *Appl. Phys. Lett.* **2001**, *78*, 1068.

10.1021/cm0606124 CCC: $33.50
Published on Web 11/08/2006

are required,[14] resulting in sintering of the particles and correspondingly low surface areas (normally around 20−50 $m^2\ g^{-1}$), which is a great disadvantage as far as applications in catalysis are concerned. Coprecipitation of hydroxides is an alternative method[15] but it is difficult to ensure that a homogeneous distribution of the metal ions in the precursor, which ensures crystallization of small spinel particles during the calcination, is obtained. Spinel materials with high specific surface areas can be obtained by calcining precursors prepared by sol−gel processes[3b] since the slow gel formation process allows the metal cations to become uniformly distributed. This method has some drawbacks however in that the precursors, typically metal alkoxides, are both expensive and difficult to handle on a large scale.

Herein we report a self-generated templating pathway for the synthesis of high-surface-area mesoporous $ZnAl_2O_4$ spinels. The key feature of this strategy is that the templates are self-generated and no preformed templates are involved in the synthesis system. One recent publication describes the synthesis of hollow carbon nanospheres and carbon nanocapsules by pyrolysis of ferrocene. Since a single precursor is both the source of the carbon and the templates, the latter were described as self-generated template.[16] Another feature of our self-generated templating approach is use of a *single-source* inorganic precursor, Zn−Al layered double hydroxide (ZnAl-LDH). LDHs are synthetic layered anionic clays[17] in which the metal ions are bonded to hydroxyl groups to form two-dimensional brucite-like layers that are stacked together through electrostatic interactions between interlayer anions and positively charged layers. Within the layers, the cations are *uniformly distributed on an atomic level* without segregation of "lakes" of separate cations.[18] Calcination of LDHs is known to give spinels but these are always mixed with the oxide of the divalent metal.[17] This reflects the fact that, in LDHs, the ratio M^{II}/M^{III} is typically[17] in the range 2−4 whereas in a spinel the required ratio is $M^{II}/M^{III} = 0.5$. However, we recently found that when appropriate amounts of Fe^{2+} are incorporated into the brucite-like layers of Fe^{3+}-containing LDHs, pure MFe_2O_4 spinel ferrites (M = Mg, Co, and Ni) can be obtained.[19] In addition, in the case of M^{II} = Zn, the amphoteric nature of ZnO formed in calcined ZnAl-LDH allows it to be extracted by alkali. Selective leaching of ZnO from the decomposition product of a single-source precursor has also been reported to obtain a macroporous NiO monolith.[20] The large amount of ZnO in our approach therefore effectively acts as a self-generated template to direct the formation of high-surface-area spinel with an interconnected mesopore network. The process is illustrated schematically in Figure 1. In this paper, we focus on a detailed study of the textural and morphological properties of the resulting $ZnAl_2O_4$ spinels to understand the nature of the established synthetic approach. In addition, due to the high surface areas exhibited by the as-prepared $ZnAl_2O_4$ spinels, their photocatalytic activities for wet oxidation of phenol have also been examined under UV irradiation. To the best of our knowledge, no report has been published on the photocatalytic degradation of phenol over zinc aluminate.

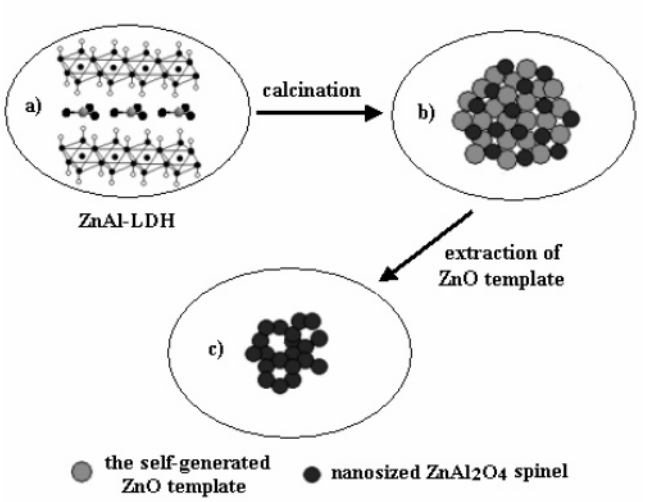

Figure 1. Schematic illustration of the synthesis of mesoporous $ZnAl_2O_4$ spinel with high specific surface area through a self-generated template pathway with ZnAl-LDH as a single-source precursor: (a) a *single-source* ZnAl-LDH precursor; (b) in the process of calcination, the newly formed $ZnAl_2O_4$ spinel nanocrystallites were confined in the voids formed by the self-generated highly dispersed ZnO template, thereby avoiding the growth of large spinel particle; (c) after removal of the self-generated ZnO template by selective leaching, $ZnAl_2O_4$ spinel with unusually high specific surface area and a mesopore network (see Figure 6) is obtained.

Experimental Section

Synthesis of Zn−Al LDH Precursor. A Zn−Al LDH precursor was prepared by a method involving separate nucleation and aging steps.[21] Solution A: $Zn(NO_3)_2{\cdot}6H_2O$ and $Al(NO_3)_3{\cdot}9H_2O$ with a Zn^{2+}/Al^{3+} molar ratio of 3.0 were dissolved in 100 mL of deionized water to give a solution with a total cationic concentration of 1.2 M. Solution B: NaOH and Na_2CO_3 were dissolved in 100 mL of deionized water to form a mixed base solution. The concentrations of the base were related to those of the metal ions in solution A as follows: $[CO_3^{2-}] = 2.0[Al^{3+}]$, $[OH^-] = 1.6([Zn^{2+}] + [Al^{3+}])$. Solutions A and B were simultaneously added rapidly to a colloid mill with the rotor speed set at 3000 rpm and mixed for 2 min. The resulting suspension was aged at 90 °C for 4 h, centrifuged, washed thoroughly with distilled water, and finally dried at 60 °C overnight. Elemental analysis: Found % (Calcd for $[Zn_{0.76}Al_{0.24}(OH)_2](CO_3)_{0.12}{\cdot}0.78H_2O$): Zn 47.31 (47.43); Al 6.23 (6.18); H_2O 12.66 (12.62); Zn/Al 3.14 (3.17).

(14) Hong, W.; De Jonghe, L. C.; Yang, X.; Rahaman, M. N. *J. Am. Ceram. Soc.* **1995**, *78*, 3217.
(15) Valenzuela, M. A.; Jacobs, J. P.; Bosch, P.; Reijine, S.; Zapata, B.; Brongersma, H. H. *Appl. Catal. A* **1997**, *148*, 315.
(16) Zou, G.; Yu, D.; Lu, J.; Wang, D.; Jiang, C.; Qian, Y. *Solid State Commun.* **2005**, *131*, 749.
(17) (a) Cavani, F.; Trifiró, F.; Vaccari, A. *Catal. Today* **1991**, *11*, 173. (b) *Layered Double Hydroxides: Present and Future*; Rives, V., Ed.; Nova Sci. Pub.: New York, 2001. (c) *Clay Surfaces: Fundamentals and Applications*; Wypych, F., Satyanarayana, K. G., Eds.; Elsevier (Academic): London, 2004. (d) *Handbook of layered materials*; Auerbach, S. M., Carrado, K. A.; Dutta, P. K., Eds.; M. Dekker Inc.: New York, 2004. (e) Evans, D. G.; Slade, R. C.T. *Struct. Bond.* **2006**, *119*, 1. (f) Li, F.; Duan, X. *Struct. Bond.* **2006**, *119*, 193.
(18) Vucelic, M.; Jones, W.; Moggridge, G. D. *Clays Clay Miner.* **1997**, *45*, 803.
(19) (a) Liu, J.; Li, F.; Evans, D.G.; Duan, X. *Chem. Commun.* **2003**, 542. (b) Li, F.; Liu, J.; Evans, D. G.; Duan, X. *Chem. Mater.* **2004**, *16*, 1597.
(20) Rajamathi, M.; Thimmaiah, S.; Morganc, P. E. D.; Seshadrib, R. *J. Mater. Chem.* **2001**, *11*, 2489.
(21) Zhao, Y.; Li, F.; Zhang, R.; Evans, D. G.; Duan, X. *Chem. Mater.* **2002**, *14*, 4286.

Synthesis of $ZnAl_2O_4$ Spinel. Samples of the above-synthesized Zn−Al LDH (Zn/Al = 3.0) precursor were calcined in air at 500 or 600 °C for 3 h or at 700, 800, and 1000 °C for 2 h with a heating rate of 10 °C/min. The resulting products were slowly cooled to room temperature. To remove the formed ZnO in a calcined mixture, 1.0 g of calcined materials were subsequently treated with 25 mL of aqueous sodium hydroxide solution (10 M) at 60 °C for 2 days under moderate stirring. The final products were separated by centrifugation several times and dried at 80 °C overnight. ZnAl-LDH samples calcined at 500, 600, 700, 800, and 1000 °C are denoted CL-5, CL-6, CL-7, CL-8, and CL-10, respectively; the $ZnAl_2O_4$ spinel products obtained after extraction of ZnO template from the above materials are denoted ZA-5, ZA-6, ZA-7, ZA-8, and ZA-10, respectively. Due to quite small particle size of sample ZA-5, a stable colloid solution is formed after the removal of ZnO from the calcined mixture. Therefore, after the colloid solution was placed for 3 days, sample ZA-5 was separated by centrifugation.

Characterization. Powder X-ray diffraction (XRD) patterns of the samples were collected using a Shimadzu XRD-6000 diffractometer under the following conditions: 40 kV, 30 mA, graphite-filtered Cu Kα radiation (λ = 0.15418 nm). The samples, as unoriented powders, were step-scanned in steps of 0.04° (2θ) using a count time of 10 s/step. The observed diffraction peaks were corrected using elemental Si as an internal standard [$d(111)$ = 0.31355 nm; JCPDS file no. 27-1402].

Elemental analysis was performed using a Shimadzu ICPS-7500 inductively coupled plasma emission spectrometer (ICP-ES). Samples were dried at 100 °C for 24 h prior to analysis, and solutions were prepared by dissolving the samples in dilute hydrochloric acid (1:1).

Room-temperature Fourier transform infrared (FT-IR) spectra were recorded in the range 4000 to 400 cm^{-1} with 2 cm^{-1} resolution on a Bruker Vector-22 Fourier transform spectrometer using the KBr pellet technique (1 mg of sample in 100 mg of KBr).

Thermogravimetric and differential thermal analysis (TG-DTA) were carried out in air on a Perkin-Elmer Diamond thermal analysis system with a heating rate of 10 °C/min.

^{27}Al solid-state magic-angle spinning (MAS) NMR spectra were measured on a Bruker AV300 spectrometer operating at 78.20 MHz with a pulse width of 0.5 s, spinning rate of 8000 Hz, and an acquisition delay of 0.5 μs between successive pulses to avoid saturation effects.

Transmission electron microscopy (TEM) images were recorded with Philips TECNAI-20 and JEOL JEM-2010 high-resolution transmission electron microscopes. The accelerating voltage was 200 kV.

The specific surface area determination and pore volume and size analysis were performed by BET and BJH methods using a Quantachrome Autosorb-1C-VP Analyzer. Prior to the measurements, samples were degassed at 200 °C for 2 h.

Photocatalytic Reactions. The photocatalytic activities for wet oxidation of phenol over $ZnAl_2O_4$ spinels were performed in a quartz reactor at ambient temperature. The UV source was two 36 W H-type lamps (Beijing electric light sources research institute) with a maximum emission at approximately 254 nm. Typically, an aqueous phenol solution (100 mg/L, 200 mL) containing 0.2 g of catalyst was vigorously stirred and irradiated by UV light for 3 h. The initial concentration of phenol was chosen according to that of contamination to be dealt with in wastewater.[22] The phenol conversion and product distribution were determined by HPLC. Aliquots of 5 μL were injected into a reverse-phase C-18 column, with a mixture of 30% methanol and 70% of redistilled water as a mobile phase at a total flow rate of 0.8 mL/min. The absorbance at 280 nm was used to measure the distributions of products.

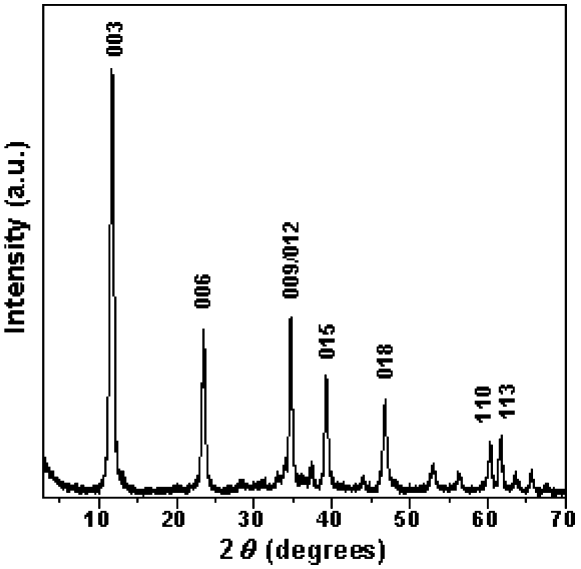

Figure 2. Powder XRD pattern of the ZnAl-LDH precursor.

Results and Discussion

Preparation and Characterization of the LDH Precursor. A ZnAl-LDH with interlayer carbonate anions was prepared by a method developed in our group involving separate nucleation and aging steps,[21] which facilitates the large-scale synthesis of LDH nanomaterials with smaller and more uniform crystallite size than can be obtained using conventional coprecipitation techniques. A Zn/Al ratio of 3.0 was employed in the synthesis mixture. The powder XRD pattern of the as-prepared ZnAl-LDH (Figure 2) exhibits the characteristic diffraction peaks of a well-crystallized hydrotalcite-like LDH material (JCPDS file no. 38-0486)[23] with a series of (00*l*) harmonics at low angle corresponding to a basal spacing of 7.552 Å; no other crystalline phases are present. On the basis of elemental analysis as well as thermogravimetric (TG) analysis, the proposed chemical composition of the precursor is $[Zn_{0.76}Al_{0.24}(OH)_2](CO_3)_{0.12}\cdot 0.78H_2O$], indicating that the Zn/Al ratio in the precursor is similar to that in the initial synthesis mixture.

Preparation of $ZnAl_2O_4$ Spinel. Figure 3 shows the powder XRD patterns of the ZnAl-LDH precursor calcined at different temperatures. Heating at 500 °C destroys the layered structure and the characteristic X-ray diffraction peaks of ZnO (zincite) and $ZnAl_2O_4$ spinel phases appear simultaneously and become sharper as the calcination temperature is increased to 800 °C, indicative of a concomitant increase in their crystallite sizes. LDHs possess several advantages as a precursor to spinels.[19,24] A uniform distribution of metal cations on the atomic level in the brucite-like layers without segregation of "lakes" of separate cations facilitates the crystallization of a spinel phase upon calcination. The close structural relationship between the LDH

(22) Vandevivere, P. C.; Bianchi, R.; Verstracte, W. *J. Chem. Technol. Biotechnol.* **1998**, *72*, 289.

(23) Busetto, C.; Del Piero, G.; Mamara, G.; Trifiró, F.; Vaccari, A. *J. Catal.* **1984**, *85*, 260.

(24) Bellotto, M.; Rebours, B.; Clause, O.; Lynch, J.; Bazin, D.; Elkaim, E. *J. Phys. Chem.* **1996**, *100*, 8535.

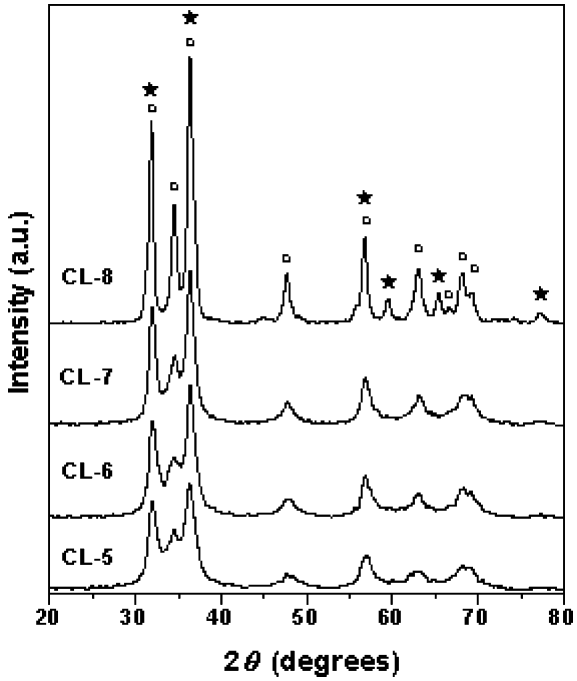

Figure 3. Powder XRD patterns of ZnAl-LDH calcined at different temperatures (the notation CL-X indicates the calcination temperature was X00 °C); (○) ZnO zincite; (★) $ZnAl_2O_4$ spinel.

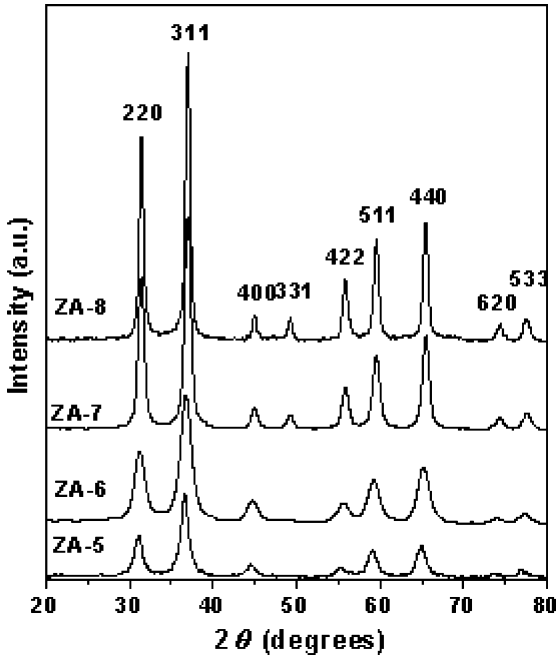

Figure 4. Powder XRD patterns of $ZnAl_2O_4$ spinels obtained by calcination of an LDH precursor at different temperatures followed by removal of ZnO by selective leaching (the notation ZA-X indicates the calcination temperature was X00 °C).

precursor and its calcination product is also a key factor. The formation of a spinel from an LDH has been described as a topotactic process in which the (110) reflection of the LDH transforms to the (440) reflection of the spinel.[24] Furthermore, the fact that the spinel is produced from a single-source precursor rather than a physical mixture means that the calcination process requires a lower temperature and shorter time, leading to a lower chance of side reactions, such as volatilization of zinc oxide, which would give nonstoichiometric or mixed products.[11]

The resulting calcined ZnAl-LDHs were subsequently treated with aqueous alkali solution, followed by extensive washing with water. The powder XRD patterns of the treated solids (Figure 4) reveal that the ZnO phase has been completely removed and that only the spinel phase remains. Elemental analysis gives Zn/Al ratios of 0.52−0.54, which confirms that removal of the ZnO phase is essentially complete. All diffraction peaks can be indexed to the $ZnAl_2O_4$ spinel structure. The measured lattice parameter a of the $ZnAl_2O_4$ spinels is 0.8088 ± 0.0012 nm, in good agreement with the reported value (0.8085 nm, JCPDS no. 05-0669). The presence of the spinel type structure is also confirmed by FT-IR spectroscopy (not shown), as there are three typical characteristic absorption peaks[12] at around 500, 560, and 670 cm^{-1}.

^{27}Al Solid-State NMR Spectroscopy. ^{27}Al MAS NMR spectroscopy is an extremely sensitive probe of the coordination environment of aluminum[25] and can provide an excellent means to investigate the site occupancy of Al^{3+} cations.[12,26] Octahedral Al^{3+} ions give resonance with chemical shifts in the range −20 to 10 ppm, while those for tetrahedral Al^{3+} centers occur between 50 and 80 ppm.[27] $ZnAl_2O_4$ spinel, which has a face-centered cubic oxide lattice with two lattice sites available for cation occupancy, may be written as $(Zn_{1-\gamma}Al_{\gamma})[Zn_{\gamma}Al_{2-\gamma}]O_4$, where the round and square brackets denote cation sites with tetrahedral and octahedral coordination, respectively, and γ represents the degree of inversion. The ^{27}Al MAS NMR spectra of the $ZnAl_2O_4$ spinel products are shown in Figure 5. The presence of both tetrahedral AlO_4 sites (chemical shift at ∼ 65 ppm) and octahedral AlO_6 sites (chemical shift at ∼5 ppm) is unequivocally demonstrated. For samples ZA-7 (calcined at 700 °C) and ZA-8 (calcined at 800 °C), the octahedral peak appears as a doublet. This is a result of a second-order splitting by nuclear quadrupole interactions, which indicates the highly crystalline nature of samples calcined at higher temperatures.[12] This is consistent with the XRD diffraction data described above. The extent of occupancy of tetrahedral sites by Al^{3+} cations shows a marked decrease with calcination temperature. The degree of inversion, calculated from the tetrahedral to octahedral peak area ratio, decreases monotonically with calcination temperature from $\gamma = 0.14$ for sample ZA-5 (calcined at 500 °C) to $\gamma = 0.02$ for sample ZA-8 (calcined at 800 °C). This is consistent with other studies on $ZnAl_2O_4$ prepared by conventional routes, which have shown that in well-crystalline samples the degree of inversion is very low.[11]

TEM Analysis. The morphological characteristics of the $ZnAl_2O_4$ spinels were investigated by transmission electron microscopy (TEM). As shown in Figure 6a, the small nanoparticles of sample ZA-5 obtained at 500 °C are not quite regular in shape, somewhat roughly spherical and cubic, and seem to aggregate with each other to form a three-dimensional network with abundant textural mesopores. This

(25) Dumeignil, F.; Rigole, M.; Guelton, M.; Grimblot, J. *Chem. Mater.* **2005**, *17*, 2361.
(26) Meyer, F.; Hempelmann, R.; Mathur, S.; Veith, M. *J. Mater. Chem.* **1999**, *9*, 1755.
(27) Morey, O.; Goeuriot, P. *J. Eur. Ceram. Soc.* **2005**, *25*, 501.

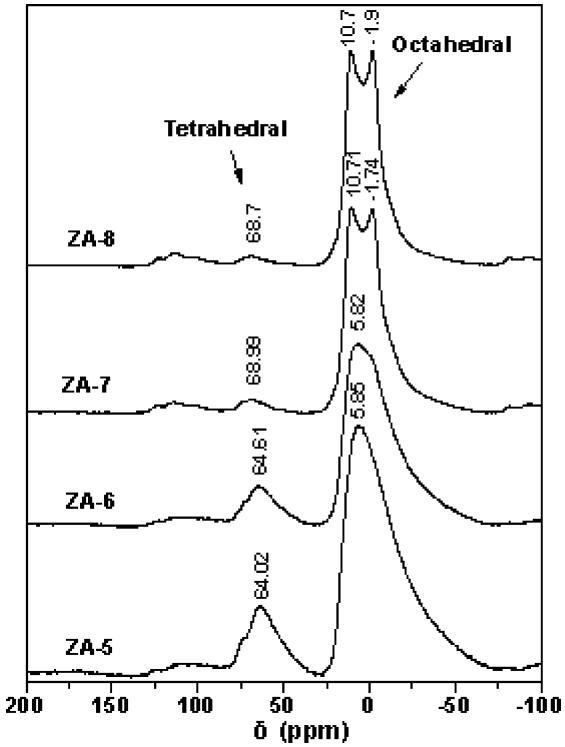

Figure 5. ^{27}Al solid-state MAS NMR spectra of $ZnAl_2O_4$ spinels obtained by calcination of an LDH precursor at different temperatures followed by removal of ZnO by selective leaching.

kind of mesostructure should be advantageous for catalytic applications from the point of view of facilitating diffusion. High-resolution TEM (HRTEM) and selected area electron diffraction (SAED) analysis provides more detailed structural information about the $ZnAl_2O_4$ spinels. Examination of the HRTEM image, shown in Figure 6b, reveals that the materials are highly crystalline, as evidenced by well-defined lattice fringes in some regions. The inset of Figure 6b shows the SAED pattern of the $ZnAl_2O_4$ nanocrystallite for sample ZA-5. All the diffraction rings can be indexed to a cubic $ZnAl_2O_4$ phase, which is consistent with the XRD results. Figure 6c shows the TEM micrograph of sample ZA-7. It can be seen that the $ZnAl_2O_4$ spinel also consists of interconnected networks of roughly spherical nanoparticles. The estimated diameters of the spherical nanoparticles vary in the range 6−11 nm, with an average of 8 nm, in good agreement with the XRD results (Table 1). Figure 6d shows a typical HRTEM image of an individual $ZnAl_2O_4$ nanocrystallite for sample ZA-7. The measured spacing of the crystallographic planes is 0.24 nm, which corresponds to the (311) lattice spacing of $ZnAl_2O_4$.

More interestingly, the TEM and XRD results reveal that when the calcination temperature is raised from 500 to 700 °C, the increase in the particle size of $ZnAl_2O_4$ nanoparticles is minimal. Meanwhile, it should be noted that the estimated amount of ZnO is 5 times that of $ZnAl_2O_4$ spinel in the calcined mixture. All this suggests that the large amount of self-generated ZnO template particle has a remarkable confined effect on the growth of $ZnAl_2O_4$ spinel. The $ZnAl_2O_4$ spinel nanoparticles were confined in the voids formed by the self-generated highly dispersed ZnO template and were prevented from recrystallizing/sintering at elevated temperatures. In the TEM image (Figure 7) of sample ZA-8, however, it can be seen that the $ZnAl_2O_4$ spinel nanoparticles have somewhat cubic rather than spherical morphology, and the particle size (~20 nm) is approximately 2−3 times larger than that in sample ZA-7. This indicates that there is partial sintering of the particles when the calcination temperature is increased from 700 to 800 °C. Furthermore, nanoparticles of sample ZA-8 seem to be no longer cross-linked with each other to form the porous structure, which is further confirmed by the nitrogen sorption isotherm measurements discussed below.

Table 1. Textural Properties of ZnAl-LDH Calcined at Different Temperatures and the Corresponding $ZnAl_2O_4$ Spinels Obtained after Extraction of ZnO from the Calcined LDHs

temperature/°C	500	600	700	800
mean crystallite size of $ZnAl_2O_4$[a]/nm	7	8	9	18
mean crystallite size of ZnO template[a]/nm	6	9	11	14
surface area[b] of calcined LDH/$m^2\ g^{-1}$	86	63	56	28
surface area[b] of $ZnAl_2O_4$/$m^2\ g^{-1}$	253	206	181	73
total pore volume of calcined LDH/$cm^3\ g^{-1}$	0.52	0.79	0.68	0.50
total pore volume of $ZnAl_2O_4$/$cm^3\ g^{-1}$	0.28	0.26	0.27	0.43
pore size[c] of $ZnAl_2O_4$/nm	3.4	4.8	5.7	18.2

[a] Mean crystallite size was determined using the Scherrer equation. [b] Surface area was calculated from the N_2 adsorption isotherm according to the BET method. [c] Pore size was calculated from the N_2 desorption branch using the BJH model.

Sorption Analysis. To further investigate the self-generated templating effect of ZnO and obtain detailed information about the textural properties before and after removal of ZnO, the materials were analyzed by nitrogen sorption measurements. As shown in Table 1, the BET specific surface area decreases markedly with increasing calcination temperature, especially at 800 °C, for samples both before and after removal of the ZnO template; this is consistent with the increase in mean crystallite size of both ZnO and spinels discussed above (Table 1).

Removal of the self-generated ZnO template leads to a large increase in surface area (161−227%), irrespective of the temperature at which the material was calcined. Particularly noteworthy is that sample ZA-5 has a surface area (253 $m^2\ g^{-1}$) which is higher than those of other $ZnAl_2O_4$ spinel products prepared using zeolite precursors[28] or sol−gel methods.[29] Moreover, even sample ZA-10 obtained at 1000 °C still has a reasonable surface area, for a spinel, of 51 $m^2\ g^{-1}$ (nitrogen adsorption isotherm not shown). [Note that spinels have higher densities than most other common solids (e.g., zinc aluminate, $\rho = 4.6$ g cm^{-3}; silica, $\rho = 2.2$ g cm^{-3}) and thus, for identical particle sizes, will have lower specific surface areas]. Besides, to investigate the influence of the amount of ZnO on the structure properties of $ZnAl_2O_4$ spinel product, $ZnAl_2O_4$ spinel was also prepared by calcining the ZnAl-LDH precursor with the initial Zn^{2+}/Al^{3+} molar ratio of 2.0. Accordingly, the estimated amount of ZnO is 3 times that of $ZnAl_2O_4$ spinel in the calcined mixture. The BET specific surface area of the obtained pure $ZnAl_2O_4$ spinel calcined at 700 °C is 137 $m^2\ g^{-1}$, smaller than that of sample ZA-7 (181 $m^2\ g^{-1}$), due to its larger mean crystallite size

(28) Schmidt, W.; Weidenthaler, C. *Chem. Mater.* **2001**, *13*, 607.
(29) (a) Valenzuela, M. A.; Boshch, P.; Aguilar-Rios, G.; Montoya, A.; Schifter, I. *J. Sol-Gel Sci. Technol.* **1997**, *8*, 107. (b) Wei, X.; Chen, D. *Mater. Lett.* **2006**, *60*, 823. (c) Areán, C. O.; Sintes, B. S.; Palomino, G. T.; Carbonell, C. M.; Platero, E. E.; Soto, J. B. P. *Microporous Mater.* **1997**, *8*, 187.

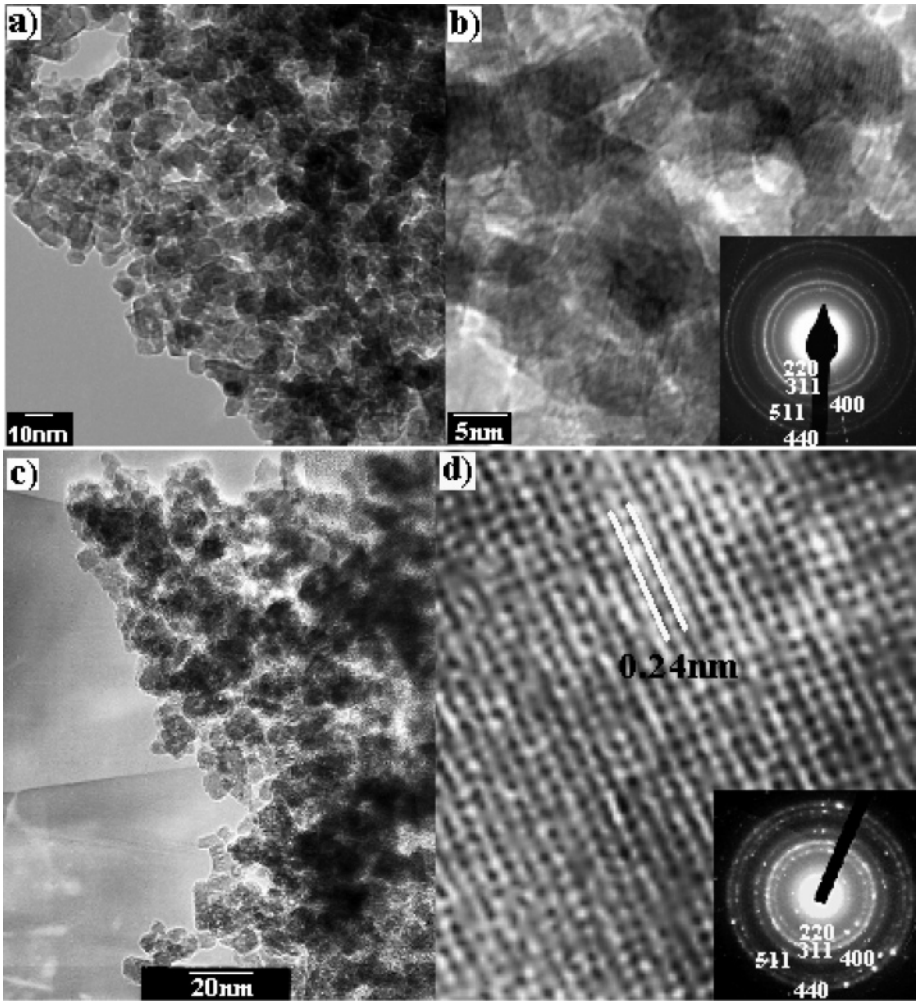

Figure 6. (a) TEM image of $ZnAl_2O_4$ spinel (ZA-5); (b) HRTEM image of $ZnAl_2O_4$ spinel (ZA-5), showing the lattice fringes of the crystalline nanoparticles and the electron diffraction pattern (inset); (c) TEM image of $ZnAl_2O_4$ spinel (ZA-7); (d) HRTEM image of $ZnAl_2O_4$ spinel (ZA-7) and the electron diffraction pattern (inset).

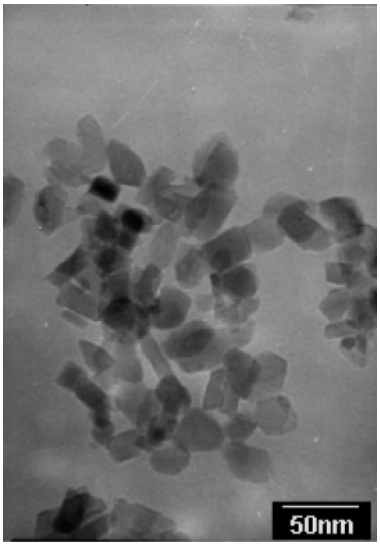

Figure 7. TEM image of $ZnAl_2O_4$ spinel (ZA-8).

(11 nm) than that of sample ZA-7 (9 nm). Therefore, it can be concluded that a smaller amount of ZnO shows a less remarkably confined effect on the growth of $ZnAl_2O_4$ spinel.

Figure 8 shows the nitrogen sorption isotherms of the calcined ZnAl-LDHs and the corresponding $ZnAl_2O_4$ spinel products. The pore size distributions (Figure 9) were determined by means of the Barrett−Joyner−Halenda (BJH) model from the desorption branches of the nitrogen sorption isotherms. Calcined ZnAl-LDHs (Figure 8a) have a type IV isotherm with a H3 type hysteresis loop that does not exhibit any limiting adsorption at high P/P_0. This is commonly observed[30] with aggregates of platelike particles giving rise to slit-shaped pores, indicating that the platelike morphology of the LDH precursor has been retained in the calcined mixture.[31] In the case of sample CL-5, there are fewer particle aggregates formed during the calcination process and corresponding particle sizes are smaller due to the relatively low calcination temperature. Therefore, the pore diameter distribution of sample CL-5 covers a narrow range (around 2−7 nm), with a maximum at ∼3.8 nm (Figure 9a). At higher calcination temperatures, calcined ZnAl-LDH display larger pore diameters and broader distributions in the range of 3−100 nm.

As expected, removal of the self-generated ZnO template leads to remarkable differences in the pore characteristics of the materials. Samples ZA-5, ZA-6, and ZA-7 (Figure

(30) Sing, K. S. W.; Everett, D. H.; Haul, R. A. W.; Moscou, L.; Pierotyi, R. A.; Rouquérol, J.; Siemieniewska, T. *Pure Appl. Chem.* **1985**, *57*, 603.
(31) Reichle, W. T.; Kang, S. Y.; Everhardt, D. S. *J. Catal.* **1986**, *101*, 352.

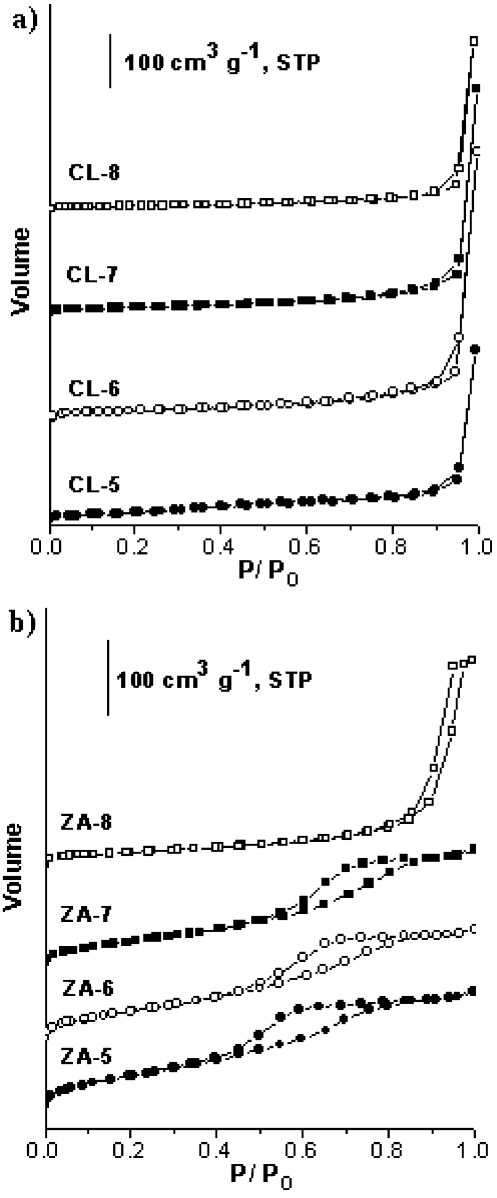

Figure 8. N_2 sorption isotherms of (a) ZnAl-LDH calcined at different temperatures and (b) corresponding $ZnAl_2O_4$ spinels obtained after extraction of ZnO from the calcined LDHs.

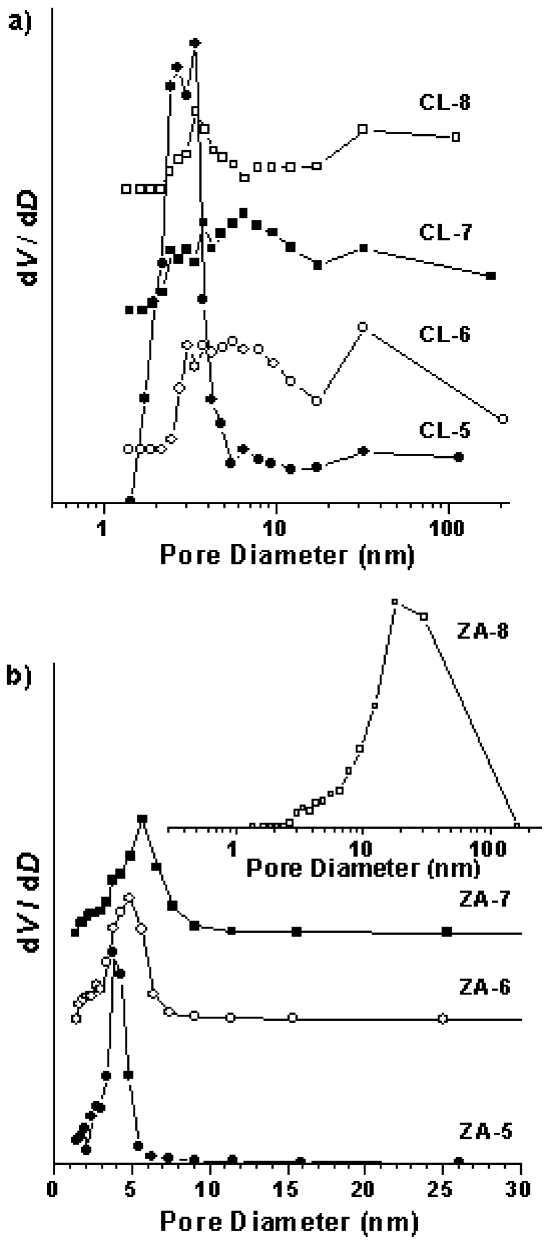

Figure 9. Pore size distributions of (a) ZnAl-LDH calcined at different temperatures and (b) the corresponding $ZnAl_2O_4$ spinels obtained after extraction of ZnO from the calcined LDHs.

8b) have type IV isotherms with pronounced H2 type hysteresis loops, which are characteristic of many mesoporous materials.[32] Taking sample ZA-7 for example, the N_2 adsorption jump in the range $P/P_0 = 0.5-0.8$ is due to the capillary condensation in the mesopores.[33] The monotonic shift of the closure points to higher relative pressure in the isotherms of samples ZA-5 to ZA-7 is indicative of an increase in the pore diameter of the samples. From the BJH pore size distributions (Figure 9b), it can be observed that larger diameter pores originally present in samples CL-5 to CL-7 disappear after removal of ZnO and the corresponding spinels exhibit only a *very narrow* pore size distribution in the range below 10 nm. This might be associated with the loss of interparticle pores as a consequence of the removal of a large amount of ZnO particles from the calcined solids. The large amount of self-generated highly dispersed ZnO template particles in calcined LDHs is very effective in separating the spinel nanocrystallites, and as a consequence of the resulting restricted recrystallization/sintering at elevated temperatures, porous $ZnAl_2O_4$ spinel products are obtained after removal of ZnO. These factors all play a role in preserving the high surface areas of the $ZnAl_2O_4$ spinel. $ZnAl_2O_4$ spinels with high surface area and narrow pore size distribution have also been prepared by sol−gel technique. Valenzuela and co-workers have reported that the sol−gel sample calcined at 600 °C for 8 h has a high surface area (171 $m^2\ g^{-1}$) with a maximum pore size at 10.1 nm.[29a] Moreover, after introduction of oxalic acid as a chelating agent in the sol−gel technique, $ZnAl_2O_4$ spinel obtained after calcination at 700 °C for 5 h shows a lower surface area (58 $m^2\ g^{-1}$) but smaller maximum pore size (2.9 nm).[29b]

(32) Leofanti, G.; Padovan, M.; Tozzola, G.; Ventureli, B. *Catal. Today* **1998**, *41*, 207.
(33) Kang, M.; Kim, D.; Yi, S. H.; Han, J. U.; Yie, J. E.; Kim, J. M. *Catal. Today* **2004**, *93*, 695.

Table 2. Conversion of Phenol and Selectivity to Oxidization Products for $ZnAl_2O_4$ Photocatalysts

sample	conversion of phenol (%)	selectivity to HQ[b] (%)	selectivity to BQ[c] (%)	selectivity to CAT[d] (%)	selectivity to oxalic acid (%)	selectivity to CO_2 (%)
$ZnAl_2O_4$[a]	55	4.9	7.3	24.2	31.1	32.5
ZA-5	69	2.6	3.4	25.2	25.2	43.6
ZA-6	68	3.2	4.6	25.4	24.9	41.9
ZA-7	66	3.6	4.1	28.3	25.7	38.3
ZA-8	65	3.8	5.5	26.1	35.1	29.5

[a] Prepared by the conventional solid-state method at 1000 °C for 12 h. [b] HQ: hydroquinone. [c] BQ: *p*-benzoquinone. [d] CAT: catechol.

Therefore, the advantage of our route is that $ZnAl_2O_4$ spinels with higher surface areas can be formed at a lower temperature and shorter calcination time without using expensive metal alkoxides compared with the sol−gel technique.

The specific surface area decreases from sample ZA-5 to sample ZA-7, whereas the pore diameters increase (see Table 1). As can be seen from the TEM image (Figure 6), the porous structure of $ZnAl_2O_4$ spinel results mainly from the aggregation of $ZnAl_2O_4$ nanopaticles. The mean crystallite sizes of $ZnAl_2O_4$ spinel estimated from the XRD patterns show a gradual increase with increasing calcination temperature (Table 1). This increase in crystallite size leads to a significant increase in pore diameter and decrease in surface area. Furthermore, it was also found that the mean crystallite size of the ZnO template (Table 1) estimated from the XRD patterns is larger than the corresponding pore diameter of the $ZnAl_2O_4$ spinel product and that a monomodal pore system (Figure 9b) is formed after removal of the ZnO template, indicating that there is a contraction of the porous structure during removal of ZnO.[6a]

The textural properties of sample ZA-8 are significantly different from those of samples ZA-5, ZA-6, and ZA-7, however. The surface area of sample ZA-8 is markedly lower (Table 1) and the nitrogen sorption isotherm is of type IV with a H1 type hysteresis loop in the relative pressure range of 0.85−0.97, which is characteristic of aggregates of larger $ZnAl_2O_4$ nanocrystallites.[32] This is consistent with the TEM observation of sample ZA-8 (Figure 7). In addition, it should be noted that the total pore volume of spinel sample ZA-8 is higher than those of the other products, mainly due to the existence of larger voids between the interconnected large particles.

Photodegradation of Phenol. $ZnAl_2O_4$ spinel is a semiconductor with the band gap of 3.8 eV.[9] So the optical adsorption threshold for $ZnAl_2O_4$ is 326.3 nm, which is within the UV range. Photocatalytic process is based on the generation electron/hole pairs by means of band gap radiation, which can give rise to redox reactions with species adsorbed on the surface of the catalysts. Therefore, it is likely that due to their high surface areas the as-prepared $ZnAl_2O_4$ spinels by LDH precursor produce a large amount of electron/hole pairs under UV irradiation with proper wavelength, and thus show good photocatalytic property.

At room temperature and atmospheric pressure, the photocatalytic activities in the degradation of phenol of the as-prepared $ZnAl_2O_4$ spinels by LDH precursor were examined. $ZnAl_2O_4$ spinel with 7 $m^2\ g^{-1}$ of specific surface area prepared by the conventional solid-state method at 1000 °C for 12 h is used here as a reference sample, making direct comparison of the catalytic activity of the two kinds of spinel materials possible. It is well-known that the degradation of phenol is thought to pass through phenyl hydroxyl compounds, binary acids and small molecular carboxylic acids, and finally CO_2. As can be seen from Table 2, all $ZnAl_2O_4$ spinels prepared by LDH precursor route show higher conversion of phenol compared with that prepared by the conventional solid-state method. The larger the surface area, the higher the conversion of phenol. Furthermore, the smaller the pore size, the higher the selectivity to CO_2. This is because that the large surface area increases the accessible number of active sites to the reactants, and the smaller pore size is advantageous to the deep oxidation of phenol.

Conclusions

A self-generated templating approach for the synthesis of $ZnAl_2O_4$ spinels with high specific surface areas of up to 253 $m^2\ g^{-1}$ and mesopore networks has been established and investigated in detail. This significant method has several advantages such as low cost and relative ease of precursors synthesis without the release of toxic or flammable gases. The use of a *single-source* ZnAl-LDH precursor is of key importance in ensuring the crystallization of a homogeneous $ZnAl_2O_4$ spinel phase, which occurs on calcination of the precursor at temperatures as low as 500 °C. This is a consequence of the uniform distribution of Zn^{2+} and Al^{3+} cations within the precursor. Meanwhile, the presence of the self-generated ZnO template in the calcined materials has been found to play a key role in generation of high surface areas, and controlled formation of mesopores with a very narrow size distribution. More interestingly, the photocatalytic results show that the formation of as-synthesized spinels with enhanced surfaces enables the development of new applications for photocatalysts with excellent structural properties, such as high thermal stability and strong resistance to acid and alkali. Moreover, such a tunable mesopore network $ZnAl_2O_4$ spinel should be desirable for various applications, such as for supports in heterogeneous catalysis, as they have very interesting textural, thermal, and structural properties. The synthesis strategy described might open a new route for fabrication of many different ceramic, spinel materials concerned with interconnected pore systems.

Acknowledgment. The authors gratefully acknowledge the financial support from the National Science Foundation of China for International Cooperation (No. 20620130108), the National Science Foundation of China (No. 20306003), and the Program for New Century Excellent Talents in University (No. NCET-04-0120).

CM0606124